Electronic structure of *N*,*N*′-ethylene-bis(1,1,1-trifluoropentane-2,4-dioneiminato)-copper(II) (Cu-TFAC), from soft X-ray spectroscopies and density functional theory calculations

A. DeMasi,[a] S. W. Cho,[a] L. F. J. Piper,[a] A. R. H. Preston,[a] K. E. Smith,*[a] R. J. Allenbaugh,[b] W. A. Barksdale[b] and L. H. Doerrer[b]

Received 11th December 2009, Accepted 19th January 2010
First published as an Advance Article on the web 10th February 2010
DOI: 10.1039/b926277f

The element and orbital-specific electronic structure of thin films of the organic material *N*,*N*′-ethylene-bis(1,1,1-trifluoropentane-2,4-dioneiminato)-copper(II) (designated as Cu-TFAC) has been studied using a combination of synchrotron radiation-excited resonant X-ray emission spectroscopy, X-ray photoelectron spectroscopy, X-ray absorption spectroscopy and density functional theory calculations. Furthermore, resonant X-ray emission at the carbon *K*-edge was used to measure the density of states for individual C sites in the molecule.

Introduction

The potential advantages of carbon-based electronic devices over those based on traditional inorganic semiconductors have motivated extensive research into the electronic structure of thin film organic semiconductors. To date, however, there is no detailed description of the relationship between the electronic structure of the molecular unit and the properties of the extended networks of molecular semiconductors. In general, the field relies on largely empirical observations to guide future studies.[1] The phthalocyanine (Pc) molecule is a ubiquitous organic electronic material since upon deprotonation, numerous metals and metal-based cations bond to the central nitrogen atoms. It would be highly advantageous to study other similar systems and develop the needed structure–property relationships, and this has prompted our focus on another Cu-containing molecule: *N*,*N*′-ethylene-bis(1,1,1-trifluoropentane-2,4-dioneiminato)-copper(II). This molecule is designated as Cu-TFAC.[2–4] The Cu-TFAC molecular structure is illustrated in Fig. 1, as are the calculated highest occupied molecular orbital (HOMO) and lowest unoccupied molecular orbital (LUMO), calculated using density functional theory (DFT). We used several criteria in selecting Cu-TFAC as a target of comparison with Cu-Pc which included (i) formal oxidation state of Cu(II) and doublet electronic ground state, (ii) ligands with aromatic structures for electronic delocalization, and (iii) similar herring-bone packing in the solid state.

We report here an extensive experimental and theoretical investigation of the electronic structure of thin films of Cu-TFAC using synchrotron radiation-excited soft X-ray emission spectroscopy (XES), soft X-ray absorption spectroscopy (XAS), and photoelectron spectroscopy, together with DFT calculations. Of particular note is the use of resonant soft X-ray emission spectroscopy (RXES). RXES is a powerful spectroscopic probe that can provide bulk-sensitive and chemical site-specific electronic structure information.[5] RXES has already proven its ability to provide detailed information regarding the states near the Fermi level (E_F) for selected organic compounds, including the metal phthalocyanines (Pc), such as Cu-Pc,[6] Sn-Pc,[7] VO-PC,[8,9] and TiO-Pc.[10]

Experimental and theoretical details

Thin films of Cu-TFAC were grown *in situ* in a custom designed ultra high vacuum (UHV) organic molecular beam deposition (OMBD) chamber (base pressure 2×10^{-9} Torr), attached to a multi-technique soft X-ray spectroscopy system, described below. The substrates were p-type Si (100) wafers, ultrasonically cleaned in acetone before introduction into the OMBD system. Once in vacuum, the substrates were sputtered with Ar^+ for 10 min and then heated to 800 °C for 10 min. A low temperature MBE-Komponenten commercial effusion cell was used to deposit Cu-TFAC onto the substrate. The

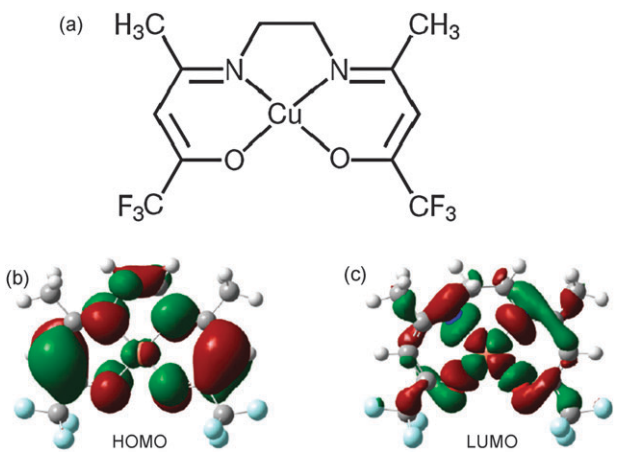

Fig. 1 (a) Schematic representations of the Cu-TFAC molecule; (b) HOMO; and (c) LUMO.

[a] *Department of Physics, Boston University, Boston, MA 02215, USA. E-mail: ksmith@bu.edu*
[b] *Department of Chemistry, Boston University, Boston, MA 02215, USA*

substrate was at room temperature during deposition. The deposition rate, monitored by a quartz crystal microbalance, was 0.03 nm s^{-1}. We found that a film of roughly 10 nm, while thick enough to mostly suppress photoemission from the Si substrate, was sufficiently thin that no charging effects were apparent during XPS studies. Thicker films did display charging during XPS measurements. The low signal strength associated with RXES experiments requires a thicker sample, but as a photon-in/photon-out spectroscopy, RXES spectra are not influenced by sample charging. The thickness of the films used in RXES measurements was typically 100–200 nm. XAS measurements of films of either thickness were found to be identical. After deposition, the samples were immediately transferred under vacuum from the OMBD chamber into the spectrometer chamber (base pressure 2×10^{-10} Torr).

All experiments were performed at the soft X-ray undulator beamline X1B at the National Synchrotron Light Source (NSLS), Brookhaven National Laboratory, which is equipped with a spherical grating monochromator. The photon beam is focused to an approximate 60×40 μm spot on the sample. X-Ray emission spectra were recorded with a Nordgren-type grazing incidence grating spectrometer.[11] XES involves the measurement of the photon emitted when a valence electron makes a radiative transition into a hole on a localized core level created by excitation of a core electron. In general, the resultant spectrum reflects the valence band density of states (DOS). Furthermore, since strong dipole selection rules govern the transition, XES directly measures the orbital angular momentum resolved DOS, *i.e.* the partial density of states (PDOS).[12,13] For example, recent studies of TiO-Pc and Alq_3 have shown that one can directly compare XES results with calculated PDOS without further considerations.[10,14] Additional information can be extracted from emission spectra if the incident monochromatic synchrotron radiation is tuned to an energy close to a core absorption threshold. This variant is referred to as RXES. In this resonant case, the excited electron resides in a conduction band or lowest unoccupied molecular orbital (LUMO) state, and the system does not become ionized. If the system exhibits core level shifts due to different chemical bonding or site symmetry, *i.e.* chemical shifts, holes can be resonantly created on each core level in turn as the excitation energy is increased, and the PDOS associated with a particular bond or chemical environment can be measured.[12]

The energy resolution for XES spectra presented here was approximately 0.4 eV near the carbon *K*-edge, and 0.6 eV near the nitrogen and oxygen *K*-edges. The energy scale of the C *K*-edge emission spectra was calibrated with 3rd order Ni L_α/L_β metal emission, while the N *K*-edge emission spectra were calibrated with 2nd order Co L_α/L_β emission, and the O *K*-edge spectra with 2nd order Zn L_α/L_β.[15] XAS spectra were recorded by the sample drain current technique to obtain the total electron yield, and were normalized to the current from an Au coated mesh, placed in the path of the incident beam. The energy scale of the XAS measurements was calibrated using known absorption features of rutile TiO_2.[16] The calibration methods for XES and XAS are consistent with each other, and confirmed by the agreement between the XES elastic peaks and the positions of chosen excitation energies on the XAS spectra. The energy resolution for XAS is approximately 0.2 eV at the carbon and nitrogen *K*-edges, and 0.3 eV at the oxygen *K*-edge. Core level XPS spectra were recorded using a Scienta 100 mm hemispherical electron analyzer, with a 0.6 eV total energy resolution for the C 1s, N 1s, and O 1s levels. Binding energies are referenced relative to the binding energy of the Au $4f_{7/2}$ core level set at 84.0 eV, as measured from a gold foil in electrical contact with the sample, with the spectra presented relative to the Fermi energy of the Au foil, which is set to zero. The total instrumental resolution of the VB-XPS, calculated from the gold Fermi edge, was determined to be approximately 0.35 eV for $h\nu = 250$ eV. DFT calculations were performed with the commercially available Gaussian 03 code.[17] Geometry was optimized and molecular orbital energies, wave functions, and charge densities were obtained using a Becke-style 3-parameters hybrid functional (B3LYP). 6-31G* Gaussian basis sets, which have given reliable results for organic materials,[18] were used. Having used this approach for Cu-TFAC, we can see from Fig. 1(b) that there is a noticeable contribution to the molecule's HOMO from the copper 3d states. Older calculations for Cu-Pc have similarly shown that its HOMO has some 3d character.[19] However, more recent theoretical studies of Cu-Pc indicate that the Cu 3d states near the Fermi level do not contribute to the molecule's HOMO.[20,21] A further study has produced a level of agreement between experiment and theory that allows for simulated XES spectra to be constructed from the DFT results.[22] In light of these recent theoretical results, we can conclude that the differing amount of 3d character in the HOMO is one of the fundamental differences in the electronic structure of Cu-TFAC and Cu-Pc. Note that the PDOS was simulated by convolving the extracted 1s and 2p energy levels with a Gaussian function with a full width at half maximum of 0.5 eV.

Results and discussion

I X-Ray photon beam induced damage

High resolution XES measurements require a small photon spot (approximately 40 μm), a high photon flux (10^{13} photons per second) on the sample, and long collection times (30–60 min). We have shown previously that these conditions lead to significant photon-induced beam damage in organic molecular thin films,[6,9] and the same has been observed for Cu-TFAC. We have solved the beam damage problem by continuously translating the films in front of the focused X-ray beam at 40 μm s^{-1}, as spectra are being recorded. This translation rate ensures spectra are recorded from pristine material every second; translating the sample more quickly yields no additional improvement in the quality of the spectra. This technique has been shown earlier to have a dramatic effect on the measured XES spectra from organic thin films.[6,10,14]

Fig. 2 compares the (a) carbon, (b) nitrogen, and (c) oxygen *K*-edge XES spectra recorded from both stationary and continuously translated Cu-TFAC films, and clearly illustrates the effect of the X-ray photon beam. The incident excitation energies were well above the ionization thresholds for each of

the corresponding 1s states. The N and O *K*-edge XES spectra from the stationary films show fewer spectral features and less definition than those from the translated films. This is an expected consequence of molecular degradation, since valence features will be particularly sensitive to any changes related to the molecular bonds. For instance, in the N *K*-edge XES measurement, significant spectral broadening is apparent following beam damage, and the pronounced peak at 395.6 eV in the spectrum from the translated film is reduced to a shoulder in the spectrum from the stationary film. This feature (marked as δ) can be identified as emission from the HOMO state, and is absent from the beam-damaged samples. For the O *K*-edge XES spectra in Fig. 2(c), the overall spectral shape is largely unchanged following beam damage, but some features are rendered absent nonetheless. The peak at 523.8 eV, for instance, is missing from the spectrum for the stationary film. Less dramatic changes between the emission from translated and stationary films are observed in the C *K*-edge XES spectra. This is due to the broad range of binding energies exhibited by the C 1s states as a result of the different local bonding environments of the C atoms (see below). The energy spread of the C 1s states means that C K_α XES spectra recorded with excitation energies far above the absorption threshold contain transitions from the valence band PDOS into a distribution of C 1s core holes, each associated with different C atomic sites. This leads to broad, relatively featureless C *K*-edge XES spectra when recorded with excitation far above threshold.

II Core level photoemission spectroscopy

Fig. 3 presents the C 1s XPS core level spectrum recorded with an incident photon energy of 425 eV. The inelastic scattered electron background has been subtracted.[23] Also shown is the calculated C 1s density of states at the C sites. To determine the precise binding energy of each site, the spectrum was fit with a number of Voigt curves. The main source of broadening is the experimental resolution (0.6 eV), so the curves are primarily Gaussian in nature. Both the peak position and area were optimized; their relative areas reflect the stoichiometry of the molecule. The calculation allows us to confidently associate four of the photoemission peaks with specific carbon atoms. The peak at 284.4 eV reflects the 1s state of carbon in a C–H environment, *i.e.* C_2 (on the adjoined methyl group) and C_4 (on the outside of the ring), while the peak at 286.1 eV is due to C_3 (C–N) and C_5 (C–O). The peaks at 285.2 eV and 292.5 eV are due to C_1 on the upper carbon bridge and C_6 on the trifluoromethyl group, respectively. Carbon atoms in environments with a higher electronegativity mismatch should have their 1s core levels shifted toward higher binding energies, and both the calculation and our measurement produce results that are consistent with this expected trend. Two additional features are also visible in the photoemission spectrum at 287.2 eV and 289.9 eV. It is likely that these are energy loss features associated with either shake-up phenomena or plasmons.[24] Such features are observed routinely in XPS from other organic systems.[10] XPS measurement of the N 1s and O 1s states (not shown) reveals, in both cases, a single spectral peak with an additional loss feature. The main XPS peaks for N 1s and O 1s are at binding energies of 399.0 eV and 531.8 eV, respectively. The loss features correspond to

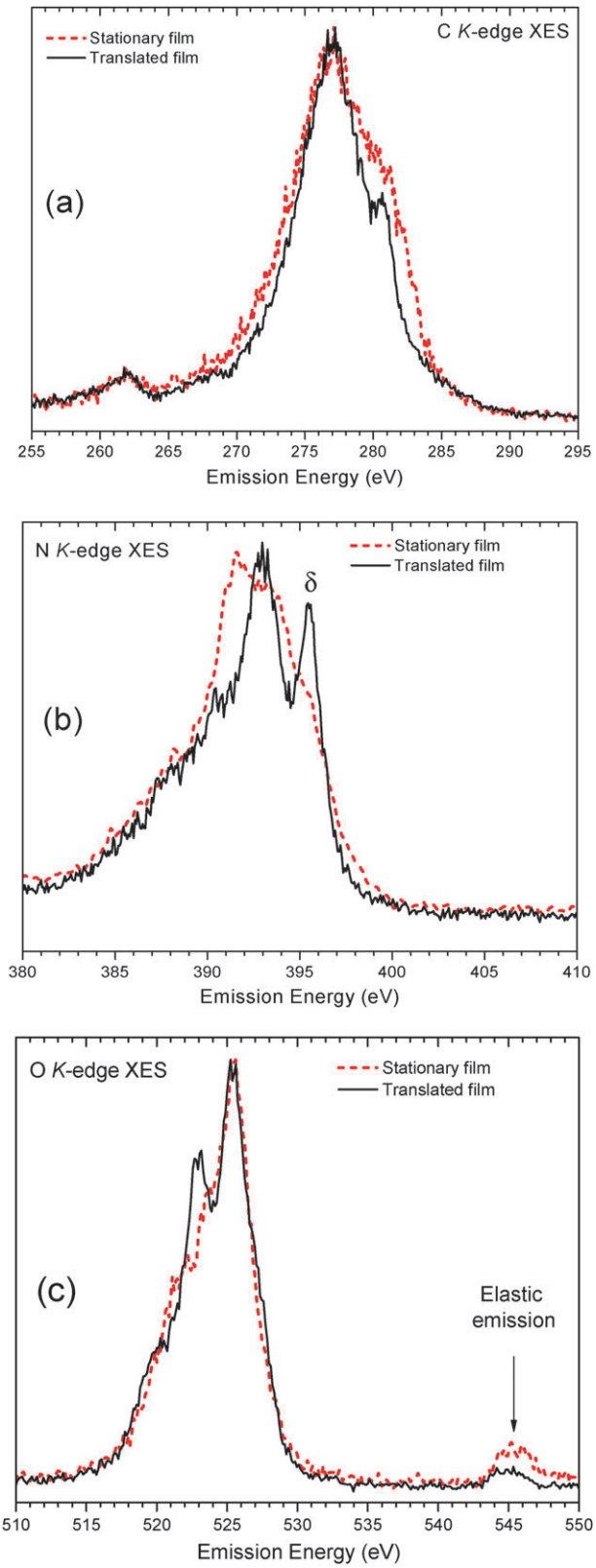

Fig. 2 The above-threshold (a) carbon, (b) nitrogen, and (c) oxygen *K*-edge XES spectra from translated and stationary Cu-TFAC films. The feature identified in (b) as δ refers to emission from the HOMO state.

energy losses of 1.2 eV for N 1s and 1.9 eV for O 1s. For both N and O *K*-edges, emission and absorption transitions involve only one core level, in contrast with the C *K*-edge where the situation is more complicated.

III C *K*-edge XES and XAS

In the upper portion of Fig. 4, the carbon *K*-edge XAS is plotted with a simulated XAS generated from the calculated unoccupied 2p PDOS for the carbon atoms. The calculated PDOS for the different atomic sites, shown in the lower portion of Fig. 4, have been shifted relative to one another by amounts corresponding to the difference in the binding energies of those sites, summed, and finally rigidly shifted to align the main feature with that of the XAS spectrum. Although XAS measures the system in an excited state, it can nevertheless generate a useful representation of the unoccupied density of states.[25] It is clear from Fig. 4 that reasonable agreement is produced between experiment and theory, allowing us to attribute XAS peaks to specific transitions on the molecule. We can reasonably conclude that the first absorption feature at 284.4 eV corresponds to 1s-LUMO transitions on the carbon atoms in a C–H environment (C_2 and C_4). Similarly, the main feature at 286.1 eV is primarily due to 1s-LUMO transitions on atoms C_3 and C_5.

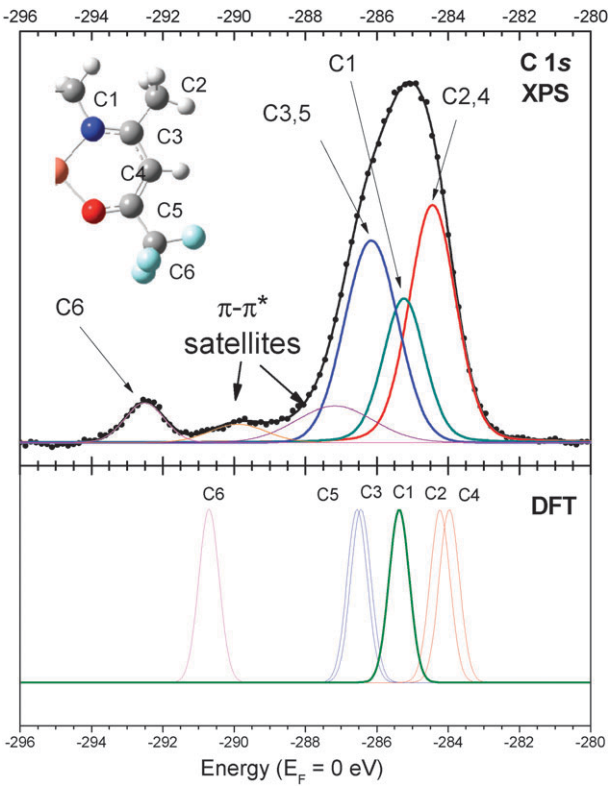

Fig. 3 Top panel: XPS spectrum of the C 1s states ($h\nu_{excite}$ = 425 eV). The inelastic scattered electron background has been removed, and the spectrum fit with six components. These were identified *via* the calculated C 1s states (bottom panel). Four distinct C 1s states can be identified, as well as two additional loss features (at 287.2 eV and 289.9 eV). A schematic representation of half of the Cu-TFAC molecule, with the various carbon environments labeled, is inset in the top panel.

Our DFT calculation also allows us to conclude that a large portion of the molecule's LUMO is localized to atoms C_3 and C_5, at least relative to its other carbon atoms. Noting the energies of the first two XAS features, and recalling the carbon 1s energies relative to the Fermi level shown in Fig. 3, it would appear that this molecule's LUMO resides precisely at E_F, and not above it as would be expected in a semiconducting molecule. This is likely the result of a final state effect associated with XAS, wherein the LUMO-excited electron is pulled toward, or even below, the Fermi energy by its Coulomb attraction to the core hole created during X-ray absorption.[26] This final state effect has been observed for thin films of other organic molecules as well, including benzene, pyridine, and Alq_3.[14,27]

Angle dependent XAS spectra were recorded at the C *K*-edge. The Cu-TFAC π bonds are oriented out of the plane of the molecule, and, due to the linear polarization of the incident X-rays, the intensity of absorption peaks due to 1s–π* transitions will change with the angle of the incidence of the photons.[26] The angular dependence of the π* absorption peaks can be used to determine the molecular orientation relative to the sample surface. For example, such XAS measurements have shown that Cu-Pc molecules do not lie flat on a Si substrate.[28] Fig. 5 shows the results of our angle resolved XAS measurements. As the angle of incidence for the photons increases from grazing, approaching normal incidence to the

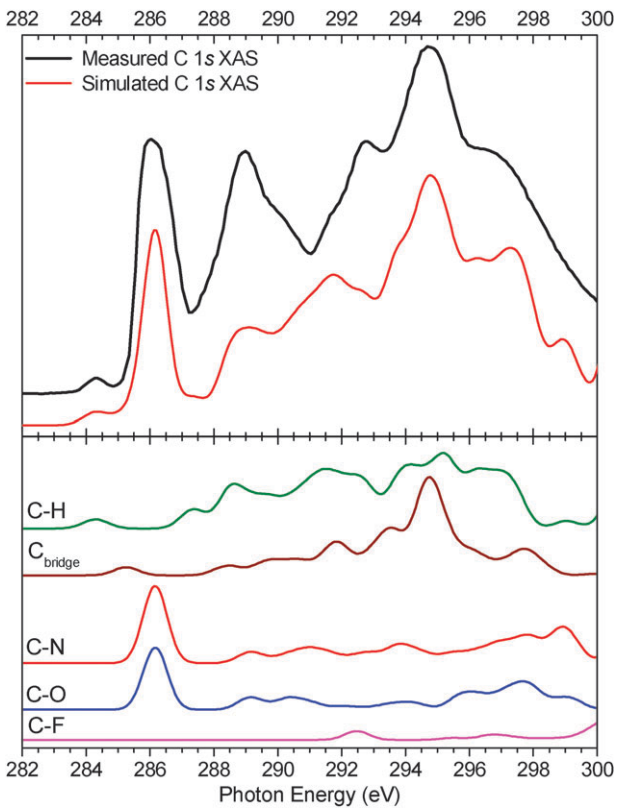

Fig. 4 Top panel: comparison of C *K*-edge XAS spectrum with the simulated XAS generated by summing the individual calculated C 2p PDOS. Bottom panel: the calculated 2p unoccupied PDOS for C atoms in each chemical environment, offset in energy according to the binding energy of their respective C 1s core states. See text.

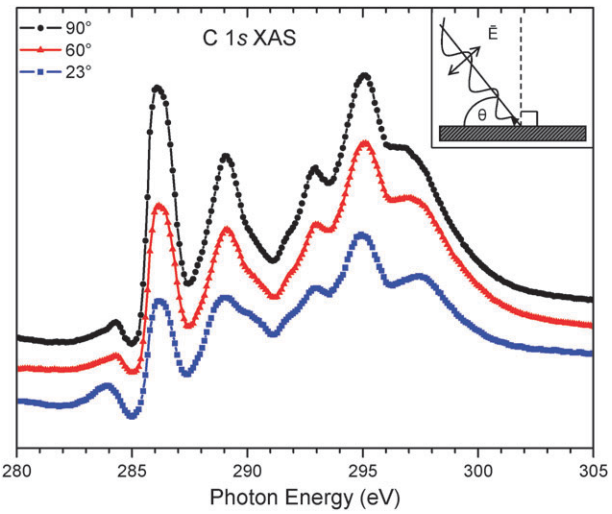

Fig. 5 C *K*-edge XAS spectra as a function of the photon angle of incidence. Spectra were recorded with the beam at 23°, 60°, and 90° relative to the surface plane. The spectral contribution from the π* orbitals increases as the photon beam goes from grazing to normal incidence. The inset shows the experimental geometry.

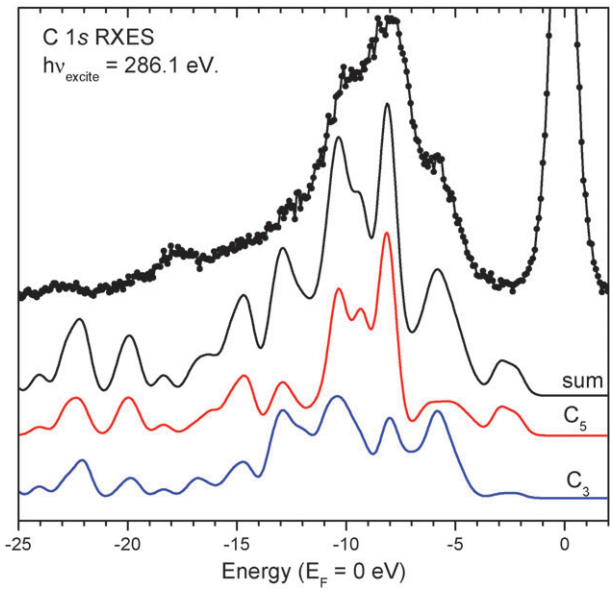

Fig. 6 Resonant C *K*-edge XES spectrum, $h\nu_{excite}$ = 286.1 eV. At this energy the emission is due primarily to 1s-LUMO transitions on the C_3 and C_5 atoms. Also shown for comparison are the calculated PDOS for the C_3 and C_5 atoms, plus a summed PDOS.

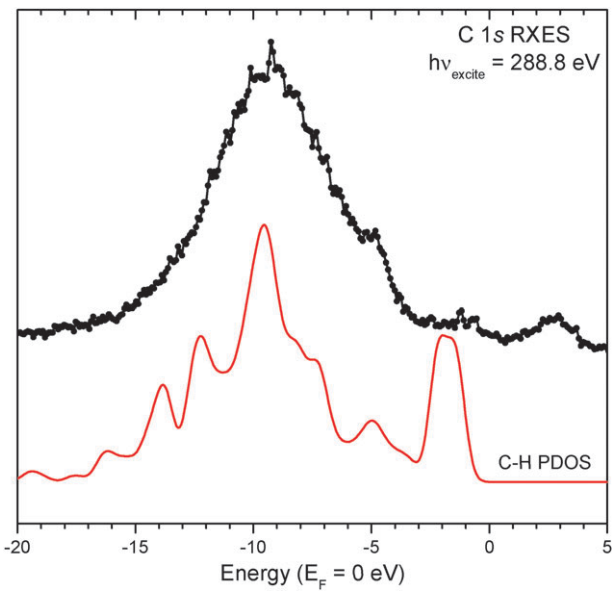

Fig. 7 Resonant C *K*-edge XES spectrum, $h\nu_{excite}$ = 288.8 eV. At this energy the emission is due primarily to excitation of the C_2 and C_4 atoms. Also shown for comparison are the calculated PDOS for the C_2 and C_4 atoms, plus a summed PDOS.

film, the contribution from the π* orbitals to the absorption also increases. This is most apparent in the feature at 286.1 eV, which has previously been assigned to a 1s-LUMO transition. This angular dependence is consistent with the molecule oriented with the molecular plane oriented approximately 70° off of the silicon substrate, an angle similar to that observed for Cu-Pc.[29] Given that the angle of molecular orientation is related to the relative strengths of molecule–substrate attraction and molecule–molecule attraction, we can reasonably conclude that Cu-TFAC has similar properties to Cu-Pc in terms of the strength of intermolecular attraction and the ability to produce ordered films.

By tuning the energy of the incident photons to a specific transition, we can choose which atoms become excited and subsequently fluoresce. Photons with an energy of 286.1 eV excite electrons into the LUMO state of atoms C_3 and C_5 only, as discussed above for Fig. 4, and so the resonant XES for this photon energy should reflect the occupied 2p PDOS of only those two carbon atoms. Fig. 6 shows the resonant X-ray emission spectrum for this energy along with the calculated occupied PDOS for C_3 and C_5. Excellent agreement is noted between experiment and theory, in terms of both the energetic locations of peaks and the overall spectral shape, although emission from the HOMO appears to be suppressed when compared to the calculation. Furthermore, the energetic location of the calculated HOMO appears shifted to higher energy relative to experiment. The large experimental peak at ~0 eV is the elastic peak for this spectrum, which is produced when the LUMO-excited electron, having just been excited from the 1s state, directly recombines with the created core hole. To produce the spectrum in Fig. 7, an excitation energy of 288.8 eV was used. This energy primarily produces transitions on atoms C_2 and C_4, the carbon atoms in a C–H environment, and so we compare the resultant emission spectrum with the calculated occupied 2p PDOS for C_2 and C_4. Once again we see good overall agreement between experiment and theory, in terms of both spectral shape and the locations of peaks, although the intensity of the DFT calculated HOMO peak again appears larger than that of the experiment as well as being shifted toward higher energy.

IV N and O *K*-edges

The N *K*-edge non-resonant XES spectra are displayed in the bottom panel of Fig. 8, together with the calculated N 2p occupied PDOS. The N *K*-edge XAS spectrum is presented,

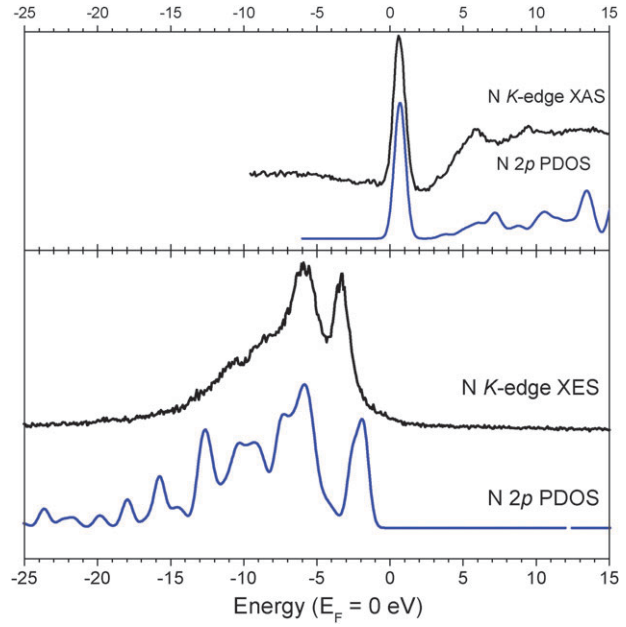

Fig. 8 Top panel: N *K*-edge XAS, along with the calculated N 2p unoccupied PDOS. Bottom panel: non-resonant N *K*-edge XES, together with the calculated N 2p occupied PDOS.

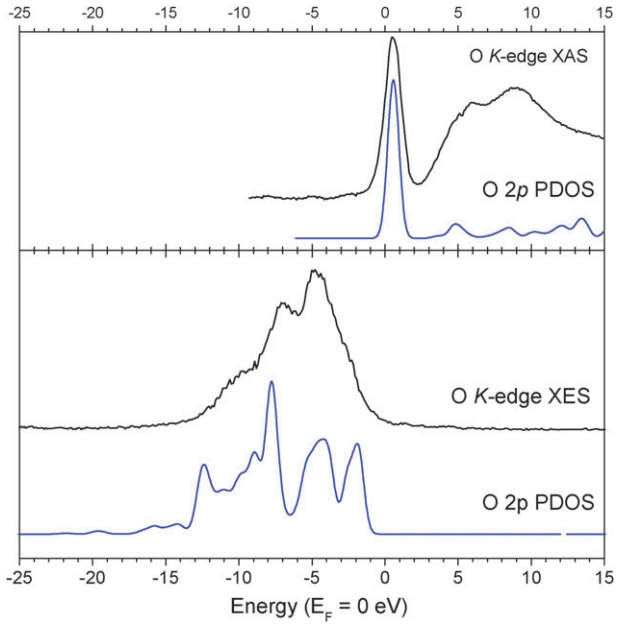

Fig. 9 Top panel: O *K*-edge XAS, along with the calculated O 2p unoccupied PDOS. Bottom panel: non-resonant O *K*-edge XES, together with the calculated O 2p occupied PDOS.

along with the calculated N 2p unoccupied PDOS, in the top panel of Fig. 8 on the same photon energy axis. A common energy scale for nitrogen emission and absorption spectra is used and referenced to E_F, corresponding to a photon energy of 399.0 eV. The intense first peak in the XAS spectrum, at about 0.6 eV, is associated with transitions from the N 1s state to the LUMO. No core level shifts are required for the calculated PDOS because there is only one nitrogen site, and hence only one binding energy for the N 1s state in the molecule. Some agreement can be seen between the measured and calculated PDOS, with the exception that the calculated energetic position of the nitrogen HOMO is notably higher than the HOMO measured with X-ray emission. This was seen earlier for the C *K*-edge, but is much more pronounced here. The O *K*-edge non-resonant XES spectra are displayed vertically offset to each other in the bottom panel of Fig. 9, together with the calculated O 2p occupied PDOS. The O *K*-edge XAS spectrum is presented, along with the calculated O 2p unoccupied PDOS, in the top panel of Fig. 9 on the same calibrated photon energy axis. E_F corresponds to an emission/absorption energy of 531.8 eV. As with the N *K*-edge, although there is some agreement between the measured and calculated PDOS, the calculated HOMO is found at a much higher energy than the HOMO measured with XES, which appears as a shoulder on the high energy side of the O *K*-edge emission spectrum. The DFT calculation, it seems, reliably miscalculates the energy for the system's HOMO state. It is most noticeable for the molecule's nitrogen and oxygen atoms, which happen to be adjacent to the central copper atoms. Spin-polarization of the central Cu atom's d states can affect the electronic structure near the Fermi level,[30] and the discrepancy in HOMO energy could be the result of an interaction with copper d-orbitals not fully taken into account by the calculation.

Conclusion

The element-specific electronic structure of the organic molecule Cu-TFAC has been studied using a combination of XES, XPS, and XAS, and compared to the results of DFT calculations. Angle resolved XAS reveals that molecules of Cu-TFAC are oriented at an angle of approximately 70° relative to the silicon substrate. The calculated N and O 2p PDOS were found to agree well with the corresponding *K*-edge resonant and non-resonant emission spectra, with the exception of the energetic location of the HOMO state. In the case of C, we have shown that by appropriately adjusting the calculated PDOS for chemical shifts, it is possible to produce a reflection of the measured spectra.

Acknowledgements

This work was supported in part by the NSF under CHE-0807368, and by the U.S. AFOSR under FA9550-06-1-0157. The NSLS is supported by the U.S. Department of Energy, Office of Science, Office of Basic Energy Sciences, under Contract No. DE-AC02-98CH10886. We thank the NSF-REU summer research program (CHE-0649114) for supporting W. A. Barksdale.

References

1 P. Cassoux and J. S. Miller, *Chem. Adv. Mater.*, 1998, 19–72.
2 H. C. Allen, Jr,, *J. Coord. Chem.*, 1975, **5**, 45–47.
3 H. C. Allen, Jr., G. L. Hillhouse and D. J. Hodgson, *Inorg. Chim. Acta*, 1979, **37**, 37–44.
4 A. E. Martell, R. L. Belford and M. Calvin, *J. Inorg. Nucl. Chem.*, 1958, **5**, 170–181.
5 A. Kotani and S. Shin, *Rev. Mod. Phys.*, 2001, **73**, 203–246.
6 J. E. Downes, C. McGuinness, P.-A. Glans, T. Learmonth, D. Fu, P. Sheridan and K. E. Smith, *Chem. Phys. Lett.*, 2004, **390**, 203–207.

7 N. Peltekis, B. Holland, L. F. J. Piper, A. DeMasi, K. E. Smith, J. E. Downes, I. T. McGovern and C. McGuinness, *Appl. Surf. Sci.*, 2008, **255**, 764.
8 Y. Zhang, T. Learmonth, S. Wang, A. Y. Matsuura, J. Downes, L. Plucinski, S. Bernardis, C. O'Donnell and K. E. Smith, *J. Mater. Chem.*, 2007, **17**, 1276.
9 Y. Zhang, S. Wang, T. Learmonth, L. Plucinski, A. Y. Matsuura, S. Bernardis, C. O'Donnell, J. E. Downes and K. E. Smith, *Chem. Phys. Lett.*, 2005, **413**, 95.
10 Y. Zhang, S. Wang, A. Demasi, I. Reid, L. F. J. Piper, A. Y. Matsuura, J. E. Downes and K. E. Smith, *J. Mater. Chem.*, 2008, **18**, 1792–1798.
11 J. Nordgren and N. Wassdahl, *Phys. Scr., T*, 1989, **31**, 103.
12 J. Nordgren and N. Wassdahl, *J. Electron Spectrosc. Relat. Phenom.*, 1995, **72**, 273–280.
13 J. Nordgren, G. Bray, S. Cramm, R. Nyholm, J. E. Rubensson and N. Wassdahl, *Rev. Sci. Instrum.*, 1989, **60**, 1690–1696.
14 A. DeMasi, L. F. J. Piper, Y. Zhang, I. Reid, S. Wang, K. E. Smith, J. E. Downes, N. Peltekis, C. McGuinness and A. Matsuura, *J. Chem. Phys.*, 2008, **129**, 224705.
15 *X-ray Data Booklet*, ed. A. C. Thompson, D. Vaughan, D. T. Attwood, E. M. Gullikson, M. R. Howells, J. B. Kortright, A. L. Robinson, J. H. Underwood, K. J. Kim, J. Kirz, I. Lindau, P. Pianetta, H. Winick, G. P. Williams and J. H. Scofield, 2nd edn, Lawrence Berkeley National Laboratory, University of California, Berkeley, CA, USA, 2001.
16 X. Chen, P. A. Glans, X. Qiu, S. Dayal, W. D. Jennings, K. E. Smith, C. Burda and J. Guo, *J. Electron Spectrosc. Relat. Phenom.*, 2008, **162**, 67–73.
17 M. J. Frisch, G. W. Trucks, H. B. Schlegel, G. E. Scuseria, M. A. Robb, J. R. Cheeseman, J. A. Montgomery, T. Vreven, K. N. Kudin, J. C. Burant, J. M. Millam, S. S. Iyengar, J. Tomasi, V. Barone, B. Mennucci, M. Cossi, G. Scalmani, N. Rega, G. A. Petersson, H. Nakatsuji, M. Hada, M. Ehara, K. Toyota, R. Fukuda, J. Hasegawa, M. Ishida, T. Nakajima, Y. Honda, O. Kitao, H. Nakai, M. Klene, X. Li, J. E. Knox, H. P. Hratchian, J. B. Cross, V. Bakken, C. Adamo, J. Jaramillo, R. Gomperts, R. E. Stratmann, O. Yazyev, A. J. Austin, R. Cammi, C. Pomelli, J. W. Ochterski, P. Y. Ayala, K. Morokuma, G. A. Voth, P. Salvador, J. J. Dannenberg, V. G. Zakrzewski, S. Dapprich, A. D. Daniels, M. C. Strain, O. Farkas, D. K. Malick, A. D. Rabuck, K. Raghavachari, J. B. Foresman, J. V. Ortiz, Q. Cui, A. G. Baboul, S. Clifford, J. Cioslowski, B. B. Stefanov, G. Liu, A. Liashenko, P. Piskorz, I. Komaromi, R. L. Martin, D. J. Fox, T. Keith, M. A. Al-Laham, C. Y. Peng, A. Nanayakkara, M. Challacombe, P. M. W. Gill, B. Johnson, W. Chen, M. W. Wong, C. Gonzalez and J. A. Pople, Gaussian, Inc., Wallingford, CT, 2004.
18 R. Q. Zhang, W. C. Lu, C. S. Lee, L. S. Hung and S. T. Lee, *J. Chem. Phys.*, 2002, **116**, 8827–8837.
19 M.-S. Liao and S. Scheiner, *J. Chem. Phys.*, 2001, **114**, 9780–9791.
20 V. Y. Aristov, O. V. Molodtsova, V. Maslyuk, D. V. Vyalikh, V. M. Zhilin, Y. A. Ossipyan, T. Bredow, I. Mertig and M. Knupfer, *Appl. Surf. Sci.*, 2007, **254**, 20–25.
21 G. Giovannetti, G. Brocks and J. van den Brink, *Phys. Rev. B: Condens. Matter*, 2008, **77**, 025133.
22 L. F. J. Piper, S. W. Cho, Y. Zhang, A. DeMasi, K. E. Smith, A. Matsuura and C. McGuinness, *Phys. Rev. B: Condens. Matter*, 2010, **81**, 045201.
23 D. A. Shirley, *Phys. Rev. B*, 1972, **5**, 4709.
24 M. Cardona and L. Ley, *Photoemission in Solids, Parts 1 and 2*, Springer Verlag, Berlin, 1978.
25 O. V. Molodtsova, M. Knupfer, V. V. Maslyuk, D. V. Vyalikh, V. M. Zhilin, Y. A. Ossipyan, T. Bredow, I. Mertig and V. Y. Aristov, *J. Chem. Phys.*, 2008, **129**, 154705.
26 J. Stöhr, *NEXAFS Spectroscopy*, Springer, Berlin, 1992.
27 J. A. Horsley, J. Stöhr, A. P. Hitchcock, D. C. Newbury, A. L. Johnson and F. Sette, *J. Chem. Phys.*, 1985, **83**, 6099–6107.
28 H. Peisert, T. Schwieger, J. M. Auerhammer, M. Knupfer, M. S. Golden, J. Fink, P. R. Bressler and M. Mast, *J. Appl. Phys.*, 2001, **90**, 466–469.
29 W. Chen, S. Chen, H. Huang, D. C. Qi, X. Y. Gao and A. T. S. Wee, *Appl. Phys. Lett.*, 2008, **92**, 063308.
30 B. Bialek, I. G. Kim and J. I. Lee, *Thin Solid Films*, 2003, **436**, 107–114.